IEEE Access
Multidisciplinary | Rapid Review | Open Access Journal

Received August 28, 2021, accepted September 20, 2021, date of publication December 13, 2021,
date of current version December 28, 2021.

Digital Object Identifier 10.1109/ACCESS.2021.3135376

Analysis of Persistent Oscillation Mechanism and Low Frequency Coupling Characteristics of Power System From the Perspective of Grid-Connected Converter

QI WANG[1], (Member, IEEE), XINGYONG ZHAO[1], AND PENG WANG[2], (Fellow, IEEE)
[1]School of Electric Power, Shanxi University, Taiyuan 030006, China
[2]School of Electrical and Electronic Engineering, Nanyang Technological University, Singapore 639798

Corresponding author: Qi Wang (343366922@qq.com)

This work was supported in part by the Science and Technology Innovation Project of Colleges and Universities in Shanxi Province under Grant 2021L005, in part by the Shanxi Province Applied Basic Research Program, Youth Project, under Grant 20210302124553, and in part by the Ministry of Education, Industry-University Cooperation and Collaborative Education Project, under Grant 202102449009.

ABSTRACT The voltage disturbance in the weak grid will cause frequency coupling and even persistent oscillation of the grid current of grid connected converter in power system. From the perspective of grid-connected converter, this paper establishes a unified complex variable model of disturbance frequency / coupling frequency in grid connected system, analyzes the evolution mechanism from SIDO (Single Input Double Output, SIDO) to DIDO (Double Input Double Output, DIDO) of grid connected converter, clarifies the relationship among voltage disturbance, grid impedance and frequency coupling. Then a robust current control strategy based on improved PLL structure has been proposed. Compared with the traditional method, this paper demonstrates that the coupling frequency component is the main cause of instability or oscillation, and the improvement of low frequency characteristics is helpful to enhance the adaptability of the converter to the weak grid. Finally, the correctness of the theoretical analysis is verified by the experimental platform.

INDEX TERMS Grid-connected converter, grid current, grid voltage, frequency coupling, robustness.

I. INTRODUCTION

With the booming proportion of distributed energy in the power system, a new generation of power system characterized by power-electronized power systems has been formed [1]. While the increasing grid-connected capacity of renewable energy and the large-scale application of power electronic equipment such as power generation and transformation units make the PCC (Points of Common Coupling, PCC) weak, which contributes to the robustness of the grid-connected converter and its adaptability to the grid [2], [3]. Having said that, the asymmetry of the control structure of the grid-connected converter becomes prominent due to the weak grid, and it may even bring hidden potential instability to the normal operation of the grid-connected system [4].

It is generally believed that the LCL-type grid-connected converter has received extensive attention and research due to its small size, low hardware cost, and good high-frequency attenuation characteristics [5]–[7]. The Converter equipped with an LCL filter will cause high-frequency resonance or even instability due to its topological structure. Amid its stability in the high-frequency domain, the conventional way tends to increase the low-frequency bandwidth to further confirm the good dynamic response characteristics of the converter [8], [9]. However, the low frequency bandwidth is mainly reflected in the current loop and the PLL (Phase Locked Loop, PLL). The dynamic response of the latter is intermediate between the voltage and current loop. If the bandwidth coefficient is large, especially when the grid voltage has low frequency disturbances, the response time scale will coincide with the current loop and cause instability [10]. In addition, the asymmetry of the PLL control structure is also one of the potential risks of system instability [11]. What's more, in early studies, PLL was often considered as the default ideal link. However, with the improvement of the performance requirements of the power system for converters and the increasing complexity of the PCC, PLL is

The associate editor coordinating the review of this manuscript and approving it for publication was Md. Apel Mahmud.

of great importance for the analysis of the stability of the grid connection system [8], [12]–[14]. The PLL was intensively considered during the modelling of converter and the parameters of the PLL were designed based on the dynamic response and stability region [8]. Ref [12]–[14] qualitatively analyzed the relationship between bandwidth and stability of PLL. Nevertheless, the two have mutual constraints in terms of performance, and it is impossible to achieve synchronization optimization of dynamic response and stability by adjusting parameters alone. The above research did not consider the effect of grid voltage disturbance on the operation status of grid-connected converters. Ref [15]–[17] pointed out that due to the asymmetry of PLL's control of PCC voltage, the grid-connected converter exhibits frequency coupling characteristics when there is a low frequency disturbance in the grid voltage (generally within 100 Hz). Under the disturbance voltage of a single frequency, the converter outputs disturbance currents of two frequencies, that is, the SIDO characteristics. The two disturbance frequencies satisfy the mirror relationship [18], [19]. In response to the above situation, relevant scholars have proposed a robust control strategy to reduce the frequency coupling effect [16], [21]–[22]. Among them, the Ref [16], [21] improved the stability of the system by constructing a voltage feedforward term, however, it did not reveal the nature of the coupling phenomenon's influence on the low-frequency characteristics and system stability. Ref [20] constructs a lead/lag link in the voltage loop so that the grid-connected converter can still ensure a higher stability margin under low-frequency voltage disturbances. However, the applicability of the stability criterion for SISO systems is questionable when grid impedances are taken into account [19].

Power system stabilizer (PSS) is widely used to suppress low-frequency oscillation phenomena [23]. The basic principle is to add a power deviation or frequency deviation signal to the voltage regulator to produce an additional torque in phase with the frequency deviation. It can increase both the damping of the unit and the damping in the system [24]. Ref [25], [26] proposed a GPSS design method based on the principle of phase compensation, which effectively suppresses the occurrence of ultra-low frequency oscillations. The mechanical damping provided by GPSS is not affected by the operating conditions of the system, nor will it deteriorate other oscillation modes in the system. It has the advantages of simple design method and suitable for on-site debugging [27], [28]. However, the above-mentioned research mainly focuses on the improvement of the power generation unit, and does not consider the coupling characteristics of the grid-connected converter.

The above research provides a good idea for solving problems such as frequency coupling of converters in weak grid. In fact, the interaction between the SIDO characteristics and the grid impedance has not been specifically analyzed, which is essential to reveal the nature of the low-frequency persistent oscillation problem in the grid-connected system. In addition, the existing research focuses on the instability and stability maintenance of grid-connected systems, with less attention paid to frequency domain analysis and its physical significance. Based on the SIDO characteristics of the grid-connected system, this paper firstly establishes a self-disturbance/mutual disturbance unified complex variable model and analyzes its frequency domain characteristics. Besides, considering the weak grid, it is revealed that the SIDO characteristics are caused by the asymmetric structure of the converter itself. The existence of grid impedance is the essence of frequency coupling, and can cause the SIDO characteristic of a grid-connected system to evolve into a DIDO characteristic. Finally, a robust current control strategy is proposed for the theoretical analysis and verified experimentally. This strategy effectively improves the low-frequency oscillation of the grid current, and improves the robustness and adaptability of the grid-connected system in a weak grid.

In summary, the limitation of the traditional method is that when PLL is considered, it is difficult to compromise the dynamic characteristics and stability of the grid-connected conversion system. At the same time, when there are uncertain voltage frequency disturbances in the grid, the coupling mechanism of the grid-connected system has not been fully revealed yet. For this, our main contributions are as follows.

1) From the perspective of grid-connected converter, this paper firstly establishes a unified complex variable model of disturbance frequency / coupling frequency in grid connected system, analyzes the evolution mechanism from SIDO to DIDO of grid connected converter.

2) Aiming at the grid-connected conversion system in a weak grid, this paper clarifies the relationship among voltage disturbance, grid impedance and frequency coupling.

3) A robust current control strategy based on improved PLL structure has been proposed. Compared to conventional methods, it is demonstrated that the coupling frequency component is the main cause of instability or oscillation, while the improved low frequency characteristics facilitate the adaptability of the converter to the weak grid. The relevant parameters are designed in detail.

II. LOW-FREQUENCY COUPLING MECHANISM OF GRID-CONNECTED CONVERTER WHEN CONSIDERING PLL STRUCTURE IN WEAK GRID

A. SIDO CHARACTERISTICS OF GRID-CONNECTED CONVERTER UNDER VOLTAGE DISTURBANCE

Fig. 1 shows the circuit model of the grid-connected system. L_1, C, and L_2 are the converter-side inductor, filter capacitor, and grid-side inductor, respectively. Z_g is the grid impedance, i_1 and i are the converter-side current and grid current, respectively. C_{dc} is the DC side capacitor, u_g is the ideal grid voltage, u_{PCC} is the voltage of PCC. R_L is the equivalent parasitic resistance of L_1 and L_2. θ is the phase information, i_{dq} and i_{dqr} are the grid current and reference current of the converter in the dq coordinate system, respectively. u_{mdq} and u_{mabc} are the modulation voltages in the dq coordinate

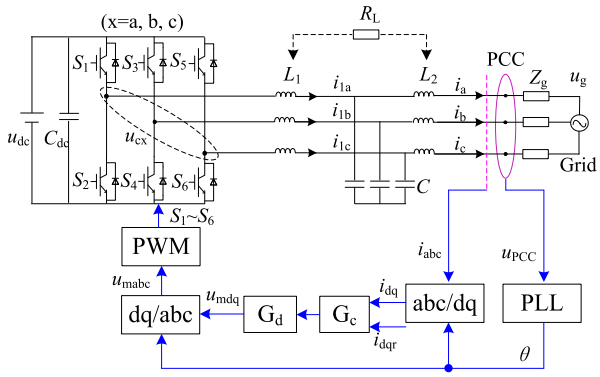

FIGURE 1. Topology of three-phase grid-connected converter.

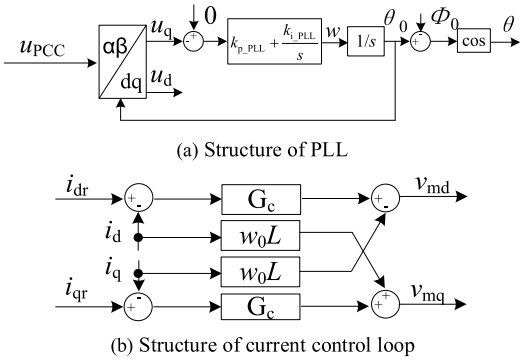

FIGURE 2. Main structure of control system.

system and abc coordinate system, respectively. $S_1 \sim S_6$ are switching signals, G_c is the current controller, and $G_d$is the delay link.

Fig. 2 is the specific control structure diagram. Fig. 2 (a) is a traditional PLL structure diagram, where k_{p_PLL} and k_{i_PLL} are PI parameters in the phase-locked loop structure, respectively. ω is the angular frequency, and Φ_0 is the power factor angle. When the disturbance is not considered, the transfer function from the q-axis voltage to the phase θ is Equation 1.

$$H_{PLL}(w) = -\frac{k_{i\_PLL} + jk_{p\_PLL}w}{w^2} \tag{1}$$

Fig. 2 (b) is the current controller structure, namely PI controller, denoted by G_c, and the expression is (2). k_p and k_i are the proportional coefficient and the integral coefficient, respectively. In the decoupling item of the figure, w_0 is the fundamental angular frequency, and L is the sum of L_1 and L_2.

$$G_c(\omega) = k_p + \frac{k_i}{j\omega} \tag{2}$$

PLL has a direct impact on the current loop in the voltage-controlled current source grid-connected converter [13]. Knowing from Fig. 2, the control structure of the PLL is characterized by the imbalance of the dq axis. When the PCC voltage has a disturbance with a frequency of w_p, denoted by V_{p,w_p}, the converter will generate a corresponding grid-connected disturbance current. Using the symmetrical component method to decompose the disturbance current, two symmetrical current components with frequencies of w_p and $2w_0 - w_p$ can be obtained, denoted by $I_{p,wp}$ and $I_{p,2w0-w_p}$ [19]. At this time, the PLL based on the dq axis asymmetric control structure depicts SIDO characteristics with the disturbance voltage. The grid current $I_s(t)$ is equation (3).

$$\dot{I}_s(t) = \dot{I}_{s,\omega_p}(t) + \dot{I}_{s,2\omega_0-\omega_p}(t) \tag{3}$$

In addition, due to the bandwidth limitation of the PLL, this feature is more sensitive to low-frequency voltage disturbances [10]. Through the admittance modeling of the grid-connected converter [18], the relationship between the input disturbance voltage and the output disturbance current can be obtained, as shown in equations (4) and (5). Among them, Y_{SA} and Y_{AA} are the self-admittance and trans-admittance (also called coupled admittance) of the grid-connected converter under disturbance voltage, respectively. In other words, the input voltage and output current of dual-frequency interference under single-frequency interference can be characterized by Y_{SA} and Y_{AA}, respectively.

$$\begin{aligned} Y_{SA}(\omega_p) &= \frac{\dot{I}_{p,\omega_p}}{\dot{V}_{p,\omega_p}} \\ &= \frac{1 - 0.5T_{PLL}(\omega_p - \omega_0)[\dot{I}_{dq}(G_c(\omega_p - \omega_0) - j\omega_0 L] \cdot}{j\omega_p L + R_L + [G_c(\omega_p - \omega_0) - j\omega_0 L] \cdot} \rightarrow \\ &\quad \leftarrow \frac{}{} \\ &\quad \leftarrow \frac{\omega_0) - j\omega_0 L)G_d(\omega_p - \omega_0) + \dot{D}_{dq}V_{dc}}{G_d(\omega_p - \omega_0)} \end{aligned} \tag{4}$$

$$\begin{aligned} Y_{AA}(\omega_p) &= \frac{\dot{I}_{p,2\omega_0-\omega_p}}{\dot{V}^*_{p,\omega_p}} \\ &= \frac{0.5T_{PLL}(\omega_0 - \omega_p)[\dot{D}_{dq}V_{dc} -}{j(2\omega_0 - \omega_p)L + R_L + (G_c(\omega_0 -} \rightarrow \\ &\quad \leftarrow \frac{(j\omega_0 L - G_c(\omega_0 - \omega_p))\dot{I}_{dq}G_d(\omega_0 - \omega_p)]}{\omega_p) - j\omega_0 L)G_d(\omega_0 - \omega_p)} \end{aligned} \tag{5}$$

In the above formulas, where I_{dq}, D_{dq}, and G_{dq} are the complex vectors of the grid-connected current under the dq axis, the duty cycle, and the equivalent delay of the control system, respectively. $V_{p,wp}{}^*$ is the conjugate component of $V_{p,wp}$. In addition, the expression of T_{PLL} is given by as follows.

$$T_{PLL}(\omega) = \frac{H_{PLL}(\omega)}{1 + V_1 H_{PLL}(\omega)} \tag{6}$$

Among them, V_1 is the effective value of the AC side voltage.

Fig.3 plots the frequency domain characteristic curves of Y_{SA} and Y_{AA} under voltage disturbance. The conventional methods ignore the SIDO characteristics caused by the inherent unbalanced structure of PLL, that is, only Y_{SA}

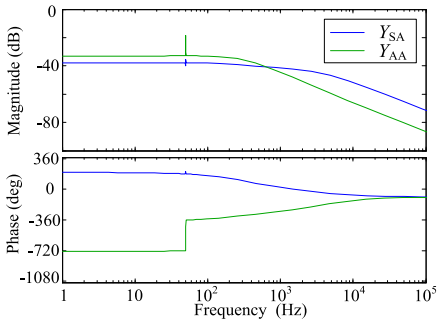

FIGURE 3. Frequency domain characteristics of Y_{SA} and Y_{AA}.

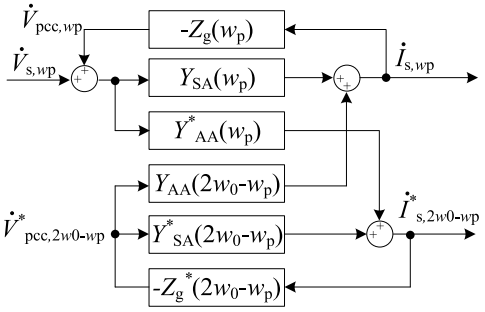

FIGURE 4. Frequency coupling mechanism diagram of grid connected converter in weak grid.

is analyzed. It can be seen from Fig. 3 that the low-frequency characteristics of Y_{AA} are similar to those of Y_{SA}. Therefore, when low-frequency disturbances in the grid-connected conversion system cause system instability, traditional analysis methods may ignore the SIDO characteristics of the grid-connected system and fail to identify the root cause of system instability, resulting in poor or even failed control strategies.

B. DISTURBANCE COUPLING MECHANISM OF GRID-CONNECTED CONVERTER IN WEAK GRID

From the above analysis, it is clear that when single frequency interference is presented in the PCC, the grid-connected converter will produce a dual frequency current response, that is, the converter exhibits SIDO characteristics. When a weak grid is considered, the SIDO characteristics will become more complicated due to the presence of grid impedance. Taking the PCC voltage as an example, I_{p,w_p} and $I_{p,2w0-w_p}$ will generate the corresponding disturbance voltages through the grid impedance, denoted by $V_{pcc,wp}$ and $V_{pcc,2w0-wp}$, respectively. That is,

$$\dot{V}_{pcc}(t) = \dot{V}_{pcc,\omega_p}(t) + \dot{V}_{pcc,2\omega_0-\omega_p}(t) \tag{7}$$

What's more, from the perspective of the circuit model, the relationship between the disturbance voltage of PCC and the disturbance current can be obtained as:

$$\dot{V}_{pcc,\omega_p} = \dot{V}_{s,\omega_p} - \dot{I}_{s,\omega_p} Z_g(\omega_p) \tag{8}$$

$$\dot{V}_{pcc,2\omega_0-\omega_p} = -\dot{I}_{s,2\omega_0-\omega_p} Z_g(2\omega_0-\omega_p) \tag{9}$$

Combining equations (4)-(5), the expressions of grid-into disturbance current with respect to converter admittance and disturbance voltage of PCC can be obtained:

$$\dot{I}_{s,\omega_p} = Y_{SA}(\omega_p)\dot{V}_{pcc,\omega_p} + Y_{AA}(2\omega_0-\omega_p)\dot{V}^*_{pcc,2\omega_0-\omega_p} \tag{10}$$

$$\dot{I}_{s,2\omega_0-\omega_p} = Y_{SA}(2\omega_0-\omega_p)\dot{V}_{pcc,2\omega_0-\omega_p} + Y_{AA}(\omega_p)\dot{V}^*_{pcc,\omega_p} \tag{11}$$

According to (8)-(11), the frequency coupling mechanism diagram of the grid-connected converter under voltage disturbance can be obtained in the grid-connected system under weak grid as follows.

From the above analysis, it is clear that the unbalanced structure such as PLL in the grid-connected converter is one of the reasons for their SIDO characteristics. At the same time, the grid impedance causes the disturbance current to form a disturbance voltage corresponding to the SIDO characteristic, the disturbance voltage then acts on the grid-connected converter, forming a frequency coupling between the disturbance voltage and the disturbance current. At this point, the grid-connected system shows the external characteristics of the DIDO. Therefore, in a weak grid, the grid impedance is the cause of frequency coupling, making the SIDO characteristics of the grid-connected converter aggravate or even runs in DIDO state. This deteriorates the robustness of the grid-connected converter, and seriously threatens the stable operation of grid-connected system.

C. STABILITY ANALYSIS

According to Fig. 1 and Fig. 4, it can be obtained that under voltage disturbance, the admittance model denoted by $Y_{inv}(w_p)$ of the converter considering the frequency coupling effect is:

$$Y_{inv}(\omega_p) = \frac{\dot{I}_{s,\omega_p}}{\dot{V}_{s,\omega_p} - \dot{I}_{s,\omega_p} Z_g(\omega_p)} = Y_{SA}(\omega_p) - \frac{Y_{AA}(2\omega_0-\omega_p)Y^*_{AA}(\omega_p)Z^*_g(2\omega_0-\omega_p)}{1+Y^*_{SA}(2\omega_0-\omega_p)Z^*_g(2\omega_0-\omega_p)} \tag{12}$$

According to the impedance stability criterion, the equivalent open-loop transfer function of the converter can be obtained. The formula is as follows, where T_0 is the open-loop transfer function of the system when the frequency coupling effect is not considered, and T is the open-loop transfer function of the system when the frequency coupling effect is considered.

$$T_0(\omega_p) = Y_{SA}(\omega_p)Z_g(\omega_p) \tag{13}$$

$$T(\omega_p) = Z_g(\omega_p)[Y_{SA}(\omega_p) - Y_{AA}(2\omega_0-\omega_p) \cdot \frac{Z^*_g(2\omega_0-\omega_p)Y^*_{AA}(\omega_p)}{1+Z^*_g(2\omega_0-\omega_p)Y^*_{SA}(2\omega_0-\omega_p)}] \tag{14}$$

Based on the two formulas above, the Nyquist diagram of the grid-connected converter when the frequency coupling effects are considered in the weak grid is obtained, as shown

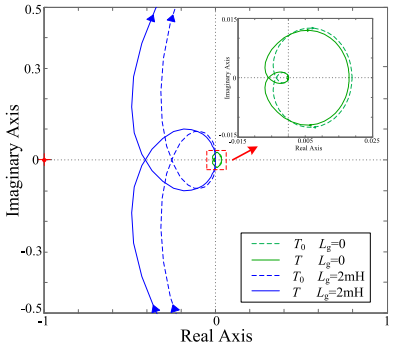

FIGURE 5. The Nyquist curve of system impedance considering frequency coupling characteristics under ideal grid and weak grid.

in Fig. 5. The dotted line is the case where frequency coupling is not considered, and the solid line is the case where coupling is considered. When L_g is 0, that is, under strong grid conditions, the Nyquist curve of the open-loop transfer function is far away from (-j,0) regardless of whether the frequency coupling effect is considered. Although the curve is closer to (-j,0) than that of frequency coupling considered, the system is still sufficiently stable. When L_g is not zero, it can be seen from the figure that the two curves move rapidly to the left, with the same trend for T_0 and T are the same, indicating that the existence of L_g has a significant effect on the frequency coupling characteristics. When the degree of weak grid is further enhanced, that is, when L_g becomes larger, the Nyquist curve of the system may surround the point of (-j,0), and the system is unstable. Therefore, the increase of the grid impedance can elevate the degree of frequency coupling, especially when the grid voltage is disturbed, the robustness of the grid-connected converter will be challenged.

III. THE PROPOSED ROBUST CURRENT CONTROL STRATEGY BASED ON IMPROVED PLL STRUCTURE

A. THE PROPOSED STRATEGY

To address the above problems, a robust current control strategy is proposed in this paper to improve the low frequency characteristics of grid-connected converters in weak grid, thereby improving the stability of the system. It can be seen from equations (13) and (14) that after considering the frequency coupling effect, the stability of the system is mainly related to the grid equivalent impedance, current controller, and PLL. Among them, the equivalent impedance of the grid is related to the capacity of the grid-connected equipment in the grid-connected system, the number of phases (single-phase or three-phase), and the effective value of the AC side voltage [18], [19], which depends on the system configuration and external control method. The design of the current controller is concerned with the bandwidth of the control system. It is not desirable to increase the phase margin of the system by reducing the low frequency gain of the current controller. Therefore, reconfiguration and design of the PLL is a more appropriate method.

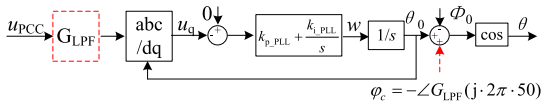

FIGURE 6. The improved PLL structure.

As frequency coupling mainly affects the low-frequency characteristics of the grid-connected system, a cascaded structure of LPF and PLL is designed in this paper. In order to avoid the phase lag caused by the LPF at the fundamental frequency, the fundamental frequency phase compensation is performed at the phase lock angle. As shown in Fig. 6.

In Fig. 6, the general expressions of LPF and Φ_c are:

$$G_{\mathrm{LPF}} = \frac{\omega_n^2}{s^2 + 2\xi\omega_n \cdot s + \omega_n^2} \tag{15}$$

$$\varphi_c = -\angle G_{\mathrm{LPF}}(j \cdot 2\pi \cdot 50) \tag{16}$$

Among them, w_n is the resonant angular frequency, and ξ is the damping coefficient. The specific values are shown in Table 1. At this point, the improved PLL transfer function is:

$$H_{PLL\_robust}(s) = G_{LPF}(s) \cdot H_{PLL}(s) \cdot e^{\phi_c} \tag{17}$$

B. PARAMETERS DESIGN

From Fig. 5 and the Ref [9, 22], it can be seen that as the grid impedance increases, the low frequency impedance curve at 200∼250Hz first appears potential instability. Considering the cross-cutting frequency of the grid impedance and the converter impedance, the frequency is generally contained in the frequency domain within 1kHz [11], and the relevant parameters of the LPF are designed as critical values at 250Hz as an example in this paper. The impedance characteristics at this frequency leave enough phase margin, thus improving the adaptability of the converter over a wide range of impedance variations. In addition, PLL mainly acts in the low-frequency domain, and has less influence on high-frequency damping suppression and current loop control. As a result, the filter capacitor can be approximately ignored. At the same time, the gain of the current controller G_c is much greater than that of PLL controller. Therefore, the output impedance of the converter can be equated to [22] without considering disturbances.

$$Z_{inv}(s) \approx -\frac{G_d(s)}{H_{PLL\_robust}(s) \cdot I_{ref}} \tag{18}$$

Combining equation (17), at 250Hz, the phase of the converter output impedance is:

$$\angle Z_{inv\_250Hz} = -180^o + \angle G_{d\_250Hz} - \angle H_{PLL\_250Hz} + (\angle G_{LPF\_50Hz} - \angle G_{LPF\_250Hz}) \tag{19}$$

As can be seen from equation (19), the first three terms of the expression are determined by the original system parameters, and the proposed strategy is mainly reflected in the latter two terms. When the latter phase is maximised,

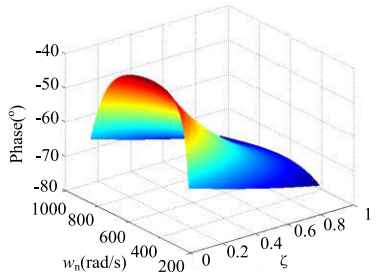

FIGURE 7. The relationship between the phase, ζ and w_n of the converter impedance.

the corresponding relevant parameter is the optimal one. Specifically, the phases of G_{LPF} at 50 Hz and 250 Hz are:

$$\begin{cases} \angle G_{LPF\_50Hz} = -\arctan[\dfrac{200\pi\cdot\xi\cdot w_n}{w_n^2-(100\pi)^2}] \\ \angle G_{LPF\_250Hz} = -\arctan[\dfrac{1000\pi\cdot\xi\cdot w_n}{w_n^2-(500\pi)^2}] \end{cases} \tag{20}$$

Substituting formula (20) into formula (19):

$$\begin{aligned} \angle Z_{inv\_250Hz} = {} & \angle G_{d\_250Hz} - \angle H_{PLL\_250Hz} \\ & - \arctan[\frac{200\pi\cdot\xi\cdot w_n}{w_n^2-(100\pi)^2}] \\ & - \arctan[\frac{1000\pi\cdot\xi\cdot w_n}{w_n^2-(500\pi)^2}] \end{aligned} \tag{21}$$

It is not difficult to see that the phase of the converter output impedance at 250 Hz is related to w_{n} and ζ in the LPF. By designing for w_{n} and ζ, the optimal phase value can be determined. Find the partial derivative of equation (21):

$$\begin{aligned} \frac{\partial(\angle Z_{inv\_250Hz})}{\partial w_n} = {} & -\frac{\frac{200\pi\cdot\xi}{(100\pi)^2-w_n^2}+\frac{400\pi\cdot\xi\cdot w_n^2}{[(100\pi)^2-w_n^2]^2}}{\frac{4\cdot(100\pi)^2\cdot\xi^2\cdot w_n^2}{[(100\pi)^2-w_n^2]^2}+1} \\ & -\frac{\frac{1000\pi\cdot\xi}{(500\pi)^2-w_n^2}+\frac{2000\pi\cdot\xi\cdot w_n^2}{[(500\pi)^2-w_n^2]^2}}{\frac{4\cdot(500\pi)^2\cdot\xi^2\cdot w_n^2}{[(500\pi)^2-w_n^2]^2}+1} \end{aligned} \tag{22}$$

According to (22), when the independent variable w_{n} is 332.01rad/s, the partial derivative is 0 and it is a concave function. Therefore, the phase of Z_{inv} has a maximum at the cutoff angular frequency. At this point, the phase value of the corresponding impedance can be obtained from ζ. Figure 7 shows the three-dimensional relationship diagram of the converter impedance phase angle, ζ, w_{n}:

It can be seen from Fig. 7 that when w_{n} is kept at its maximum value, the phase of the impedance model increases as ζ decreases. A too small ζ is likely to lead to under-damping of the LPF and cause instability. Suppose the phase of the converter impedance at 250Hz is not less than $\Phi_{\min}$, and $\Phi_{\min} > -90°$. When w_{n} takes the maximum value, according to formula (19), the converter phase expression after adopting the proposed strategy is:

$$\angle Z_{inv\_250Hz} = -\angle H_{PLL\_250Hz} - 2\arctan(\sqrt{3}\xi) \tag{23}$$

Then the expression of ζ can be obtained:

$$\xi = \frac{\tan[(-\angle H_{PLL\_250Hz} - \varphi_{\min})/2]}{\sqrt{3}} \tag{24}$$

In this paper, taking $\Phi_{\min}$ as $-60°$ as an example [4], we can calculate that ζ is 0.64.

C. STABILITY ANALYSIS

After adopting the proposed strategy, the formula (6) is:

$$T_{\mathrm{PLL\_robust}}(\omega) = \frac{H_{\mathrm{PLL\_robust}}(\omega)}{1+V_1 H_{\mathrm{PLL\_robust}}(\omega)} \tag{25}$$

Then self-admittance and mutual admittance are:

$$\begin{aligned} & Y_{\mathrm{SA\_robust}}(\omega_{\mathrm{p}}) \\ & = \frac{\dot{I}_{\mathrm{p},\omega_{\mathrm{p}}}}{\dot{V}_{\mathrm{p},\omega_{\mathrm{p}}}} = \frac{1-0.5T_{\mathrm{PLL\_robust}}(\omega_{\mathrm{p}}-\omega_0)[\dot{I}_{dq}(G_{\mathrm{c}}(\omega_{\mathrm{p}}- \rightarrow}{\mathrm{j}\omega_{\mathrm{p}}L+R_{\mathrm{L}}+[G_{\mathrm{c}}(\omega_{\mathrm{p}}-\omega_0)-\mathrm{j}\omega_0 L]\cdot} \\ & \leftarrow \frac{\omega_0)-\mathrm{j}\omega_0 L)G_{\mathrm{d}}(\omega_{\mathrm{p}}-\omega_0)+\dot{D}_{dq}V_{\mathrm{dc}}}{G_{\mathrm{d}}(\omega_{\mathrm{p}}-\omega_0)} \end{aligned} \tag{26}$$

$$\begin{aligned} & Y_{\mathrm{AA\_robust}}(\omega_{\mathrm{p}}) \\ & = \frac{\dot{I}_{\mathrm{p},2\omega_0-\omega_{\mathrm{p}}}}{\dot{V}^*_{\mathrm{p},\omega_{\mathrm{p}}}} = \frac{0.5T_{\mathrm{PLL\_robust}}(\omega_0-\omega_{\mathrm{p}})[\dot{D}_{dq}V_{\mathrm{dc}}- \rightarrow}{\mathrm{j}(2\omega_0-\omega_{\mathrm{p}})L+R_{\mathrm{L}}+(G_{\mathrm{c}}(\omega_0- } \\ & \leftarrow \frac{(\mathrm{j}\omega_0 L-G_{\mathrm{c}}(\omega_0-\omega_{\mathrm{p}}))\dot{I}_{dq}G_{\mathrm{d}}(\omega_0-\omega_{\mathrm{p}})]}{\omega_{\mathrm{p}})-\mathrm{j}\omega_0 L)G_{\mathrm{d}}(\omega_0-\omega_{\mathrm{p}})} \end{aligned} \tag{27}$$

The following picture shows the bode diagram of $Y_{\mathrm{SA\_robust}}$ and $Y_{\mathrm{AA\_robust}}$ after adopting the strategy:

In this figure, the Y_{SA} and Y_{AA} before the strategy adopted in Figure 3 are retained. When the strategy is adopted, the admittance $Y_{\mathrm{SA\_robust}}$ and mutual admittance $Y_{\mathrm{AA\_robust}}$ of the grid-connected system are indicated by dotted lines. It can be seen that the frequency domain characteristics of Y_{SA} and Y_{AA} in the low frequency band are improved after the adoption of the strategy. For Y_{SA}, the characteristics remain essentially unchanged before and after the strategy, indicating that the strategy will not affect the characteristics of the grid-connected converter. For Y_{AA}, the amplitude-frequency characteristics are significantly reduced after the strategy is adopted the coupling degree of disturbances is alleviated, the phenomenon of continuous oscillation is improved, and the grid-connected converter shows strong robustness.

Further, the open-loop transfer function of the grid-connected conversion system with this strategy is obtained as:

$$T_{0\_robust}(\omega_{\mathrm{p}}) = Y_{\mathrm{SA\_robust}}(\omega_{\mathrm{p}})Z_{\mathrm{g}}(\omega_{\mathrm{p}}) \tag{28}$$

$$\begin{aligned} T_{robust}(\omega_{\mathrm{p}}) = {} & Z_{\mathrm{g}}(\omega_{\mathrm{p}})[Y_{\mathrm{SA\_robust}}(\omega_{\mathrm{p}})-Y_{\mathrm{AA\_robust}}(2\omega_0-\omega_{\mathrm{p}}) \\ & \cdot \frac{Z^*_{\mathrm{g}}(2\omega_0-\omega_{\mathrm{p}})Y^*_{\mathrm{AA\_robust}}(\omega_{\mathrm{p}})}{1+Z^*_{\mathrm{g}}(2\omega_0-\omega_{\mathrm{p}})Y^*_{\mathrm{SA\_robust}}(2\omega_0-\omega_{\mathrm{p}})}] \end{aligned} \tag{29}$$

According to the above two formulas, strategy before and after the Nyquist curve of the grid-connected system can be obtained, as shown in Figure 9.

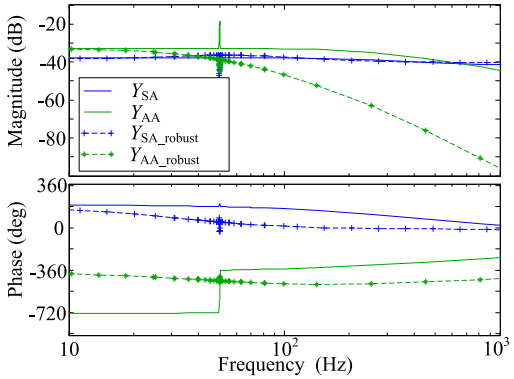

FIGURE 8. Y_{SA} and Y_{AA} with the proposed strategy.

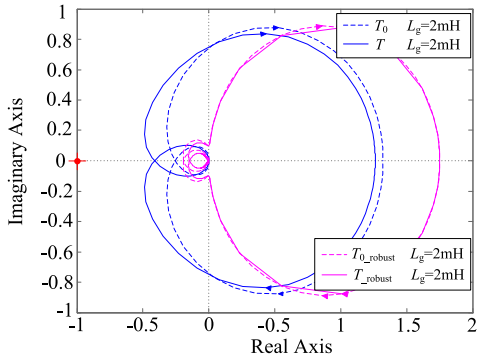

FIGURE 9. Nyquist curve of grid connected system with the proposed strategy.

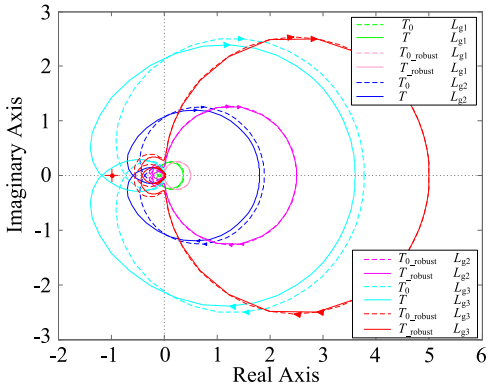

FIGURE 10. When L_g changes, the Nyquist curve of grid connected system.

In Figure 9, the blue curve is the case without the strategy, and the purple curve is the case with the strategy. Compared with Figure 5, the Nyquist curve of the grid-connected system is significantly farther away from the right-hand (-j, 0) point when this strategy is used, and the stability of the system is significantly improved. In addition, the T_{0_robust} and T_robust curves almost coincide, indicating that after the strategy is adopted, the stability of considering coupling and not considering coupling is similar, which greatly improves the instability caused by frequency coupling. In addition, the corresponding Nyquist curve can be obtained when L_g changes, as shown in Figure 10. L_{g1}, L_{g2}, and L_{g3} are 2mH, 5mH, and 15mH, respectively.

When the proposed strategy is not adopted, the Nyquist curve of the grid-connected system gradually shifts left as L_g increases. As L_g further increases further to a very small value of SCR, Nyquist shifts around (-j,0), and the system becomes unstable. With this strategy, the Nyquist curve shifts to the right, away from (-j,0), and the system regains stability. Although the increase in L_g causes the curve to shift left with the proposed strategy, compared to this case without the strategy, the grid-connected converter is able to accommodate fluctuations over a larger range of Lg and still maintain strong robustness and good adaptability to the uncertain operating of the weak grid.

IV. CASE STUDIES

A. SIMULATION RESULTS

Based on Matlab/Simulink+PLECS software, the main circuit is built in PLECS, and the control circuit is built in Simulink. The operation of the grid-connected system under two disturbance voltages is considered as shown in Fig. 11. In Fig. 11(a) and Fig. 11(b), the traditional control strategy is adopted during 0∼1s, the proposed control strategy is adopted during 1∼2s, and the proposed strategy is enabled at 1s.

Specifically, in Fig. 11(a), a voltage disturbance of 10 Hz is applied. It is not difficult to see that the grid current distortion is more serious under the voltage disturbance. The FFT analysis shows that in addition to the fundamental frequency component, the grid current mainly contains 10Hz and 90Hz components, namely the disturbance frequency and the coupling frequency, and the coupling frequency, what really matters on the quality of the grid current. This is consistent with the theoretical analysis in Fig. 3.

With this strategy, the grid current quality is restored to a three-phase highly sinusoidal waveform as shown in the Fig. 11 (a). Through the analysis of FFT, the components of the coupling frequency are greatly suppressed by FFT analysis. This shows that the coupling component caused by the coupling admittance plays vital roles in the current quality of the grid-connected system and even the stability of the grid-connected system. At the same time, for the low-frequency characteristics, it also shows that the similarity between mutual admittance (or coupled admittance) and self-admittance (or disturbance admittance) can change the low-frequency characteristics of the entire grid-connected converter, and its influence cannot be ignored. This is also consistent with the analysis in section 1.1. Similarly, we can analyze Fig.11 (b), which is not be discussed in detail here.

B. EXPERIMENTAL RESULTS

The experimental platform is shown in Fig. 12, with the dSPACE 1104 as the main processor, and K75T60 IGBT produced by Infineon as the converter switching tube.

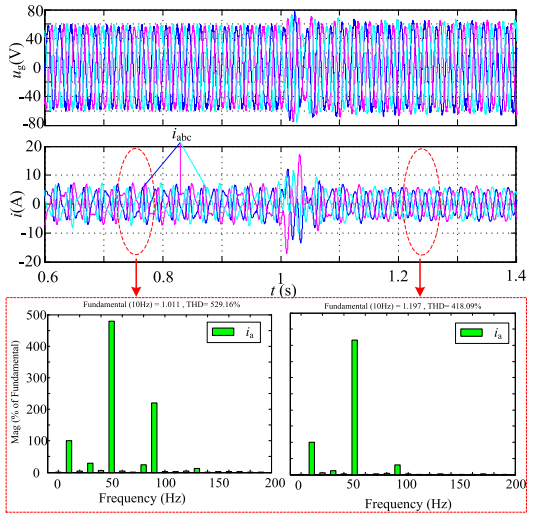

(a) Operating conditions of grid-connected system under 10Hz disturbance voltage

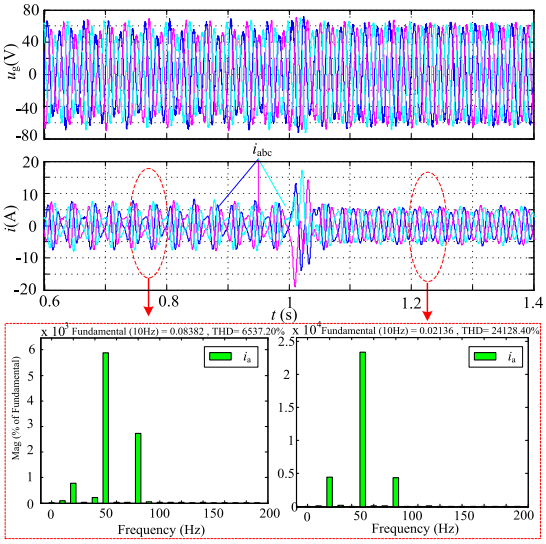

(b) Operating conditions of grid-connected system under 90Hz disturbance voltage

FIGURE 11. Waveforms of PCC under two voltage disturbance conditions.

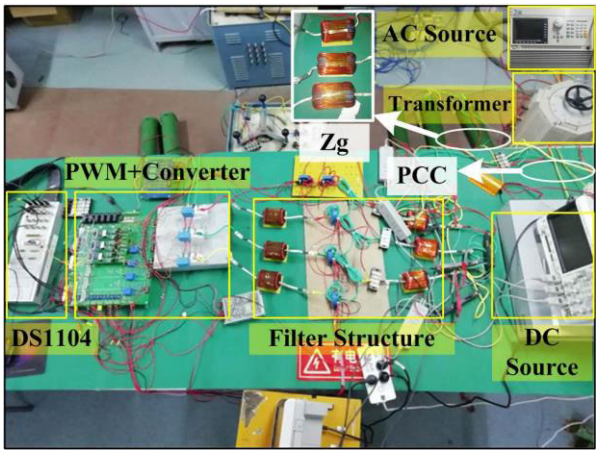

FIGURE 12. Hardware structure of the experimental platform.

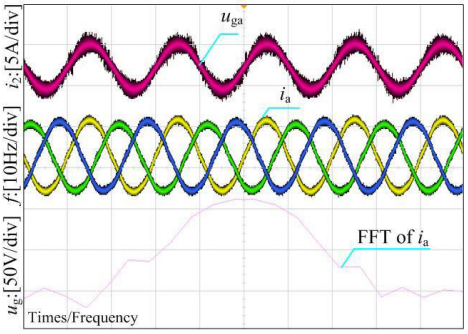

FIGURE 13. The waveform of the PCC under the ideal grid condition.

TABLE 1. Parameters of grid-connected conversion system.

Parameters	Value	Parameters	Value
U_g	80V	K_p	0.12
L_1	1.5mH	K_i	53
L_2	1.5mH	k_{p_PLL}	15
C	10uF	k_{i_PLL}	32
U_{dc}	200V	L_g	0~15mH
f_{sw}	15kHz	f_s	15kHz

The AC and DC sources are simulated by 61511 and 62150H-1000 models produced by Chroma, respectively. The current sampling is performed with LEM LV28-P and LEM LT208-S7/SP1 Hall current sensors. An Agilent series MSO-X-3054A oscilloscope is used for measurement. The experimental parameters are given in Table 1. In the experiment, the rated capacity of the grid-connected converter is 2.4kVA. The maximum current of the DC power supply is 10A. The maximum voltage of the DC power supply is 600V. The AC source is used to simulate the power grid and absorb the power of the grid-connected converter. For safety reasons, we set the rated current in the experiment to 5A.

Fig. 13 shows the waveforms of the voltage and current at PCC when the traditional control strategy is used in an ideal power grid, and FFT analysis is performed on i_a. The scales for voltage, current and frequency are on the left side of the figure. It can be seen that when there is no disturbance in the grid-connected voltage, the grid-connected current is three-phase symmetrical and highly sinusoidal.

The frequency spectrum of i_a is mainly 50Hz, indicating that the control effect is good.

When the grid voltage has a disturbance of 20 Hz, the waveform of the PCC is shown in Fig. 14. Where, Fig. 14(a) shows the voltage and grid current, and Fig. 14(b) shows the FFT spectrum corresponding to i_a at this point. It can be seen from the figure that the grid current also oscillates accordingly under the influence of the grid voltage disturbance. The oscillation is mainly concentrated at two frequencies, 20 Hz and 80 Hz. In addition, 20Hz is the disturbance frequency. Due to the asymmetry of the control structure, the grid-connected system is characterized by

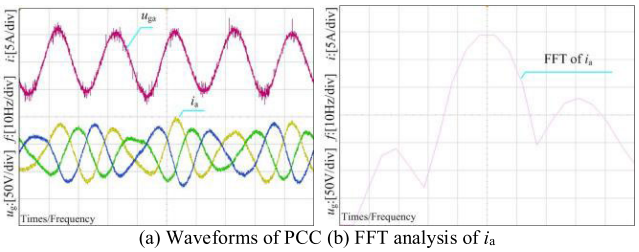

(a) Waveforms of PCC (b) FFT analysis of i_a

FIGURE 14. The voltage and current at PCC point, and FFT analysis of i_a with the traditional strategy.

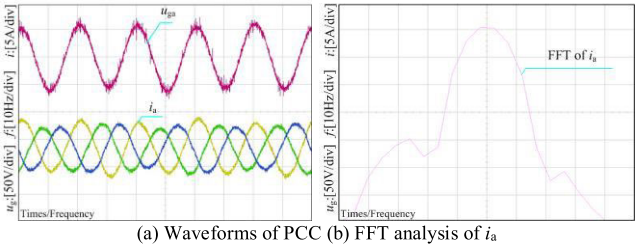

(a) Waveforms of PCC (b) FFT analysis of i_a

FIGURE 15. The voltage and current at PCC point, and FFT analysis of i_a with the proposed strategy.

SIDO characteristics. 80Hz is the coupling frequency, which is consistent with the theoretical analysis in the second section above.

When the proposed robust current control strategy is adopted, the waveform of the PCC is shown in Fig. 15. Fig. 15(a) shows the voltage and current waveforms at PCC with the proposed strategy, and Fig. 15(b) shows the FFT analysis results of i_a. It can be seen that compared to Fig. 14(a), the persistent oscillation phenomenon of the grid current has been significantly improved, and the three-phase current is highly sinusoidal. According to the analysis result of Fig. 15(b), the current content of 80Hz frequency is obviously reduced, which shows that the coupling frequency effect is the cause of the persistent oscillation of the grid-connected system. With this proposed strategy, the low-frequency characteristics of the control system are improved, so that the grid-connected converter remains strong robustness under grid voltage disturbances.

Furthermore, in order to verify the transient characteristics of the proposed strategy, Fig. 16 shows the operating conditions when the load suddenly increases from 50% to 75%. Fig. 16(a) shows the global waveforms of the voltage and current at the PCC point, while Figure 16(b) shows the local waveforms at the transient moments. It can be seen that when the load switches or the current changes suddenly, the overshoot of the grid current is small and stable, and there is no risk of instability. It shows that the strategy has good dynamic characteristics during the transient response.

Fig. 17 shows the voltage and current waveforms at the PCC when the grid impedance L_g increases to 5mH under the same grid conditions. Compared with Fig. 14, the PCC voltage has a serious disturbance, and the grid current has a more obvious low-frequency oscillation, and it runs in

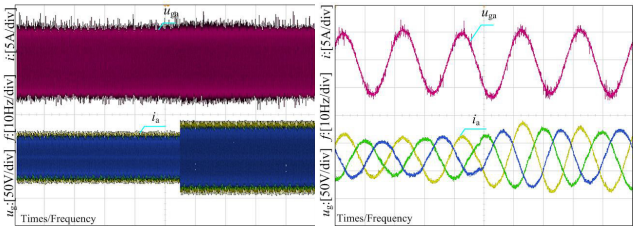

(a) Overall waveform (b) Partial waveform

FIGURE 16. Transient response of sudden current increase with the proposed strategy.

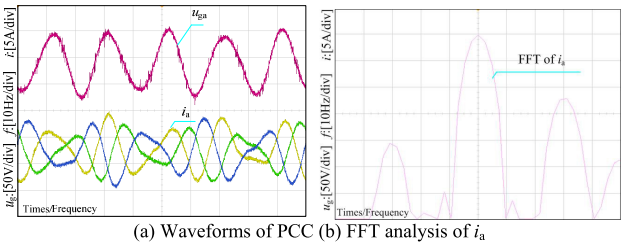

(a) Waveforms of PCC (b) FFT analysis of i_a

FIGURE 17. The voltage and current at PCC point, and FFT analysis of i_a with the traditional strategy when L_g increased.

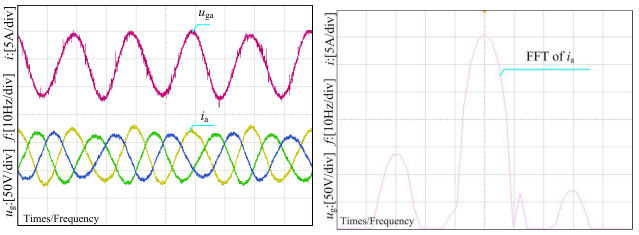

(a) Overall waveform (b) Partial waveform

FIGURE 18. The voltage and current at PCC point, and FFT analysis of i_a with the proposed strategy when L_g increased.

a persistent and periodic state. Through its FFT analysis, the current components of the disturbance frequency and the coupling frequency are more prominent, indicating that the existence of the grid impedance increases the degree of coupling, and the problem of low-frequency oscillation caused by the coupling effect becomes more complicated.

When the proposed strategy is adopted, the corresponding experimental results are shown in Fig. 18. In Fig. 18(a), the oscillation phenomenon of the grid-connected current is well improved, and the symmetrical and sinusoidal waveforms under ideal grid conditions is restored. The voltage disturbance at the PCC is also greatly reduced, and its phase is aligned with the current phase. In Fig. 18(b), the current component at the coupling frequency is reduced. The above results indicate that a weak grid increases the frequency coupling effect, which leads to severe low-frequency oscillations of the grid current. The robust current strategy proposed in this paper enhances the robustness of the grid-connected converter when the grid voltage is disturbed by improving the low-frequency characteristics of the control system. At the same time, with the increase of grid

TABLE 2. Operating conditions of grid-connected system under 10Hz disturbance voltage.

Indicators	Traditional strategy	Proposed strategy
Rise time(s)	0.237s	0.144s
Overshoots time(s)	0.167s	0.061s
Peak time(s)	0.036s	0.025s
settling time(s)	0.201s	0.119s
Proportion of disturbance frequency component in current(%)	12.35%	17.54%
Proportion of coupling frequency component in current(%)	28.4%	5.26%
THD(0.85s/1.15s, i_{abc} for example)	9.85%,10.25%,13.90%	5.72%,5.16%,6.78%
Degree of imbalance	8.43%	3.47%

impedance, the proposed strategy mitigates the frequency coupling effect and reduces grid current fluctuations, and while reducing the PCC voltage fluctuations through the grid impedance, thus also improving the voltage quality of the PCC. It has relatively satisfactory adaptability in weak grids.

C. RESULTS ANALYZED

By analyzing the results of simulation and experiment, relevant characteristic indicators can be obtained. As shown in Table 2.

Through the quantitative analysis of various indicators, we can get the following conclusions.

1) After adopting the proposed strategy, the transient characteristics of the control system such as rise time, overshoots time, peak time, and settling time have been improved. The harmonics of the grid-connected current caused by low-frequency oscillation are effectively solved, and the grid-connected current becomes highly sinusoidal. The thd results of the three-phase current changed from 9.85%, 10.25%, and 13.90% to 5.72%, 5.16%, and 6.78%. The degree of imbalance has been greatly improved, from 8.43% to 3.47%.

2) With this strategy, the content of disturbance frequency increased slightly, from 12.35% to 17.54%. However, the content of the coupling frequency is significantly reduced, from 28.4% to 5.26%. This shows that the higher coupling frequency content is the cause of the poor quality of the grid-connected current and even low frequency oscillations. Although the disturbance frequency content increases slightly, it is not the main cause of system instability. The proposed strategy can greatly reduce the coupling frequency components, effectively decouple the control system, and enhance the robustness of the grid-connected system.

V. CONCLUSION

Aiming at the persistent low-frequency oscillation of grid-connected converters in weak grids, this paper clarifies the relationship among the SIDO characteristics, grid impedance, and frequency coupling of grid-connected converters, and proposes a robust current control strategy based on improved PLL structure. The specific conclusions are as follows:

1) The asymmetric control of the voltage by the PLL structure is responsible for the SIDO characteristics of the grid-connected system when the PCC voltage is disturbed, which has little to do with the strong or weak grids. When the grid impedance is considered, the grid impedance exacerbates the SIDO characteristics and reacts to the PCC voltage, forming frequency coupling.

2) The main cause for system instability caused by frequency coupling effect is the characteristics of coupling admittance (or mutual admittance). Purposefully, the stability of the grid is greatly improved when low-frequency improvement links are applied to the grid.

3) This paper mainly focuses on the weak grid conditions with three-phase symmetrical grid impedance. In actual working conditions, the impedance of the power grid may be asymmetric. The relevant theoretical analysis will be carried out in the next study.

REFERENCES

[1] M. G. Taul, X. Wang, P. Davari, and F. Blaabjerg, "An overview of assessment methods for synchronization stability of grid-connected converters under severe symmetrical grid faults," *IEEE Trans. Power Electron.*, vol. 34, no. 10, pp. 9655–9670, Oct. 2019.
[2] Q. Wang, W. Qin, W. Dai, X. Han, L. Wang, and P. Wang, "Direct current control strategy of LCL-type converter for harmonic suppression under distorted grid condition," *IET Power Electron.*, vol. 13, no. 17, pp. 3922–3930, Dec. 2020.
[3] Q. Wang and S. University, "Robustness evaluation for harmonic suppression of LCL-type converter based on converter-side current feedback strategy under weak and distorted grid," *CPSS Trans. Power Electron. Appl.*, vol. 6, no. 2, pp. 166–177, Jun. 2021.
[4] D. Yang, X. Wang, F. Liu, K. Xin, Y. Liu, and F. Blaabjerg, "Symmetrical PLL for SISO impedance modeling and enhanced stability in weak grids," *IEEE Trans. Power Electron.*, vol. 35, no. 2, pp. 1473–1483, Feb. 2020.
[5] Q. Wang, W. Qin, L. Wang, X. Han, and P. Wang, "Robustness enhanced with damping interval widening strategy of converter equipped with an LCL filter under weak grid condition," *J. Power Electron.*, vol. 20, no. 2, pp. 410–427, Mar. 2020.
[6] W. Wu, Y. Liu, Y. He, H. S.-H. Chung, M. Liserre, and F. Blaabjerg, "Damping methods for resonances caused by LCL-filter-based current-controlled grid-tied power inverters: An overview," *IEEE Trans. Ind. Electron.*, vol. 64, no. 9, pp. 7402–7413, Sep. 2017.
[7] Y. Han, M. Yang, H. Li, P. Yang, L. Xu, E. A. A. Coelho, and J. M. Guerrero, "Modeling and stability analysis of LCL-type grid-connected inverters: A comprehensive overview," *IEEE Access*, vol. 7, pp. 114975–115001, 2019.
[8] Y. Li, X. Wang, J. Guo, H. Wu, B. Zhao, S. Wang, G. Wu, and T. Wang, "PLL synchronization stability analysis of MMC-connected wind farms under high-impedance AC faults," *IEEE Trans. Power Syst.*, vol. 36, no. 3, pp. 2251–2261, May 2021.
[9] Q. Qian, S. Xie, J. Xu, K. Xu, S. Bian, and N. Zhong, "Output impedance modeling of single-phase grid-tied inverters with capturing the frequency-coupling effect of PLL," *IEEE Trans. Power Electron.*, vol. 35, no. 5, pp. 5479–5495, May 2020.
[10] J. Xu, H. Qian, Y. Hu, S. Bian, and S. Xie, "Overview of SOGI-based single-phase phase-locked loops for grid synchronization under complex grid conditions," *IEEE Access*, vol. 9, pp. 39275–39291, 2021.
[11] H. Wu and X. Wang, "Design-oriented transient stability analysis of PLL-synchronized voltage-source converters," *IEEE Trans. Power Electron.*, vol. 35, no. 4, pp. 3573–3589, Apr. 2020.
[12] L. Yang, Y. Chen, A. Luo, Z. Chen, L. Zhou, X. Zhou, W. Wu, W. Tan, and J. M. Guerrero, "Effect of phase-locked loop on small-signal perturbation modelling and stability analysis for three-phase LCL-type inverter connected to weak grid," *IET Renew. Power Gener.*, vol. 11, no. 6, pp. 1066–1073, Set. 2019.

[13] J. Z. Zhou, H. Ding, S. Fan, Y. Zhang, and A. M. Gole, "Impact of short-circuit ratio and phase-locked-loop parameters on the small-signal behavior of a VSC-HVDC converter," *IEEE Trans. Power Del.*, vol. 29, no. 5, pp. 2287–2296, Apr. 2014.
[14] X. Zhang, S. Fu, W. Chen, N. Zhao, G. Wang, and D. Xu, "A symmetrical control method for grid-connected converters to suppress the frequency coupling under weak grid conditions," *IEEE Trans. Power Electron.*, vol. 35, no. 12, pp. 13488–13499, Apr. 2020.
[15] Y. Shen, J. Ma, L. Wang, and A. G. Phadke, "Study on DFIG dissipation energy model and low-frequency oscillation mechanism considering the effect of PLL," *IEEE Trans. Power Electron.*, vol. 35, no. 4, pp. 3348–3364, Apr. 2020.
[16] X. Zhang, D. Xia, Z. Fu, G. Wang, and D. Xu, "An improved feedforward control method considering PLL dynamics to improve weak grid stability of grid-connected inverters," *IEEE Trans. Ind. Appl.*, vol. 54, no. 5, pp. 5143–5151, Sep. 2018.
[17] Z. Shuai, Y. Li, W. Wu, C. Tu, A. Luo, and J. Z. Shen, "Divided DQ small-signal model: A new perspective for the stability analysis of three-phase grid-tied inverters," *IEEE Trans. Ind. Electron.*, vol. 66, no. 8, pp. 6493–6504, Aug. 2019.
[18] X. Zou, X. Du, G. Wang, Y. Yang, and Y. Ji, "The single equivalent inverter admittance model of three-phase grid-connected inverter system considering frequency coupling," in *Proc. 43rd Annu. Conf. IEEE Ind. Electron. Soc. (IECON)*, Oct. 2017, pp. 4994–4999.
[19] X. Du, G. Wang, Y. Shi, Y. Yang, X. Zou, H.-M. Tai, and Y. Ji, "Using asymmetric current controller to improve the stability of grid-inverter system due to PLL effect," in *Proc. IEEE 18th Workshop Control Modeling Power Electron. (COMPEL)*, Jul. 2017, pp. 1–7.
[20] X. Wu, T. Huang, X. Chen, H. Hu, and G. He, "Frequency characteristic and impedance analysis on three-phase grid-connected inverters based on DDSRF-PLL," in *Proc. 10th Int. Conf. Power Electron. ECCE Asia (ICPE-ECCE Asia)*, May 2019, pp. 1053–1058.
[21] D. Zhu, S. Zhou, X. Zou, and Y. Kang, "Improved design of PLL controller for LCL-type grid-connected converter in weak grid," *IEEE Trans. Power Electron.*, vol. 35, no. 5, pp. 4715–4727, May 2020.
[22] J. Xu, S. Bian, Q. Qian, H. Qian, and S. Xie, "Robustness improvement of single-phase inverters under weak grid cases by adding grid current feedforward in delay-based phase-locked loop," *IEEE Access*, vol. 8, pp. 124275–124287, 2020.
[23] M. J. Gibbard, Q. Zhang, and D. J. Vowles, "Electric power PSS with ramp-rejection," *IEEE Trans. Power Syst.*, vol. 35, no. 6, pp. 4495–4504, Nov. 2020.
[24] R. Jalayer and B.-T. Ooi, "Co-ordinated PSS tuning of large power systems by combining transfer function-eigenfunction analysis (TFEA), optimization, and eigenvalue sensitivity," *IEEE Trans. Power Syst.*, vol. 29, no. 6, pp. 2672–2680, Nov. 2014.
[25] J. Zhang, C. Y. Chung, and Y. Han, "A novel modal decomposition control and its application to PSS design for damping interarea oscillations in power systems," *IEEE Trans. Power Syst.*, vol. 27, no. 4, pp. 2015–2025, Nov. 2012.
[26] S. Ghosh, K. A. Folly, and A. Patel, "Synchronized versus non-synchronized feedback for speed-based wide-area PSS: Effect of time-delay," *IEEE Trans. Smart Grid*, vol. 9, no. 5, pp. 3976–3985, Sep. 2018.
[27] L.-J. Cai and I. Erlich, "Simultaneous coordinated tuning of PSS and FACTS damping controllers in large power systems," *IEEE Trans. Power Syst.*, vol. 20, no. 1, pp. 294–300, Feb. 2005.
[28] A. Dysko, W. E. Leithead, and J. O'Reilly, "Enhanced power system stability by coordinated PSS design," *IEEE Trans. Power Syst.*, vol. 25, no. 1, pp. 413–422, Feb. 2010.

QI WANG (Member, IEEE) was born in Shanyin, Shanxi, China, in 1991. He received the B.S., M.S., and Ph.D. degrees in electrical engineering from the Taiyuan University of Technology, Taiyuan, China, in 2015, 2017, and 2020, respectively. Since 2021, he has been an Assistant Professor with the School of Electric Power, Shanxi University. He is the first author of more than 15 articles. His current research interests include stability analysis of renewable energy grid grid-connected converter under complex grid conditions, power quality of micro-grid, and power system operation and control. He is currently a Reviewer of the journals *IET Power Electronics*, *Journal of Power Electronics*, *Journal of Modern Power Systems and Clean Energy*, *Proceedings of CSEE* and *et al.* He is also a Young Editorial Board Member of *Renewable Energy Resources*. He was a Branch Reporter of APECT 2018 and ICIEA 2018.

XINGYONG ZHAO received the B.Sc. and M.Sc. degrees from the Taiyuan University of Technology, Shanxi, China, in 1987, and the Ph.D. degrees from the University of Shanghai and Jiaotong University, in 2008. He is currently a Professor with Shanxi University. His current research interests include stability analysis of renewable energy grid grid-connected converter under complex grid conditions, power quality of micro-grid, and power system operation and control.

PENG WANG (Fellow, IEEE) received the B.Sc. degree from Xian Jiaotong University, Xian, China, in 1978, the M.Sc. degree from the Taiyuan University of Technology, Shanxi, China, in 1987, and the M.Sc. and Ph.D. degrees from the University of Saskatchewan, Saskatoon, Canada, in 1995 and 1998, respectively. He is currently a Life Professor with Nanyang Technological University, Singapore.